Supporting information for

Engineering Fe-N-C sites onto Fe nanoparticles for synergistically boosted Cr(VI) reduction: Performance, mechanism and application

Minghui Li,[ac] Wenjing Liu,[a] Panxinchen Liu,[a] Xiaoqin Lin,[a] Hongjie Zhu,[bc] Caixia Fang,[a] Wenwen Li[a] and Chang Liu*[a]

[a.] School of Ecology and Environment, Anhui Normal University, 189 South of Jiuhua Road, Wuhu, Anhui, 241002, P.R. China.

[b.] Shandong Provincial Key Laboratory of Chemical Energy Storage and Novel Cell Technology, School of Chemistry and Chemical Engineering, Liaocheng University, Liaocheng, Shandong, 252059, P.R. China.

[c.] State Key Laboratory of Pollution Control and Resource Reuse, School of the Environment, Nanjing University, Jiangsu, 210023, P.R. China.

*Corresponding author.

E-mail: lc2014@ahnu.edu.cn (C. Liu)

Experimental Procedures

Chemicals and Materials. All chemicals of analytic grade used in this study are listed below. $K_2Cr_2O_7$ were dried at 105 °C prior to the use. The stock solution of Cr(VI) were freshly prepared every three days with deionized water and stored at 4 °C condition.

Ferric chloride hexahydrate ($FeCl_3$•$6H_2O$), Ferric nitrate nonahydrate ($Fe(NO_3)$•$9H_2O$), Sodium persulfate ($Na_2S_2O_8$), N,N-dimethylformamide (DMF), Potassium dichromate ($K_2Cr_2O_7$, >99.5%), 2-amino-1,4-benzenedicarboxylic acid (NH_2-BDC), Benzene-1,3,5-tricarboxylic acid (H_3BTC), Methanol (CH_3OH), were purchased form Sinopharm Chemical Re agent Co., Ltd (China) and used without further purification. The grades of all chemicals above were analytical. Nano Zero Valent Iron (nZVI) was pretreated with diluted HCl solution to remove passive film. Monomeric aniline was distilled in reduced pressure before use. Hydrochloric acid (HCl), sulfuric acid (H_2SO_4), phosphoric acid (H_3PO_4) and 1,5-diphenylcarbazide were purchased from Shanghai Reagent Factory (China). Mungbean seeds were purchased from Heilongjiang Province North Pure Agricultural Products Development Co. LTD.

Synthesis of reductants. The tested reductants involved Fe_{NPs}@Fe_{SAs}NC, Fe_{NPs}/CN, Fe_{NPs}/C, Fe_{NPs}/C@Fe_{SAs}NC, nZVI@Fe_{SAs}NC, and Fe_{SAs}NC were prepared followed the previous reports combined with encapsulation- pyrolysis strategy. The details of the catalyst preparation are provided below.

The NH_2-MIL-101(Fe) was synthesized by hydrothermal method. In a typical process, a mixture solution of $FeCl_3$•$6H_2O$ (0.675 g) in DMF (7.5 mL) was added into a DMF solution of NH_2-BDC under strong stirring. After 10 min, the mixed solution was transferred to the Teflon line in a hydrothermal autoclave, heated for 24 h at 110 °C and then cooled slowly to room temperature over time. The solution was filtered, and the residual solid was washed with DMF and CH_3OH for three times, respectively. After drying under vacuum at 60 °C, a brown powder consisting of NH_2-MIL-101(Fe) was obtained. Fe_{NPs}/CN was synthesized by direct carbonization at 900 °C for 5 h under N_2 atmosphere using NH_2-MIL-101(Fe) as precursor.

Fe_{NPs}/CN@PANI was synthesized by chemical vapor deposition method (CVD). Firstly, a desired amount of Fe_{NPs}/CN was soaked by sodium persulfate solution, providing polymerization sites. Then, two quartz crucibles (one containing 1g of Fe_{NPs}/CN precursor and the other for purified aniline) were placed in a quartz tube and heated to 60 ^{o}C for 12 h simultaneously for preparing Fe_{NP}/CN@PANI. The quartz tube inlet was sealed completely and outlet port (rubber hose) was placed in water to obtain a slightly high vapor pressure. Finally, the obtained Fe_{NPs}/CN@PANI was heated at 900 ^{o}C for 5h under N_2 atmosphere. The resulting composite material was Fe_{NPs}@ Fe_{SAs}NC. For comparison, Fe_{NPs}@Fe_{SAs}NC material was washed with HCl solution (6 M) to prepare Fe_{SAs}NC material.

The synthetic method of MIL-100(Fe) was described as follows. Typically, 0.484 g of $Fe(NO_3)$•$9H_2O$ and 0.210 g of H_3BTC were dissolved to 5 mL of deionized water under stirring for 30 min. The mixture was transferred to hydrothermal autoclave, heated for 12 h at 180 ^{o}C. Then leave to cool completely, the residual solid was washed with deionized water and CH_3OH repeatedly, dried overnight. The obtained material was then heated at 900 ^{o}C for 5h under Ar atmosphere to produce Fe_{NPs}/C material. The following encapsulation-pyrolysis procedures were the same as above description. The final material was denoted as Fe_{NPs}/C@Fe_{SAs}NC. Similarly, nZVI@Fe_{SAs}NC was synthesized following above procedure using original commercial nZVI as precursor.

All obtained materials were stored in a drier without any special protection.

Reductant characterization. The physicochemical properties of the reductants were characterized using the various techniques, such as X-ray absorption fine structure spectra (XAFS), transmission electron microscopy (TEM, HAADF-STEM, EDX-mapping), atomic force microscopy (AFM), Aberration-corrected high-angle annular dark-field scanning transmission electron microscopy (AC HAADF-STEM), X-ray diffraction (XRD), N_2 adsorption-desorption measurement (BET), inductively coupled plasma spectrometry atomic emission spectroscopic (ICP-AES), X-ray photoelectron spectroscopy (XPS), Raman spectroscopy, Ultroviolet photoelectron spectroscopy (UPS), Vibrating sample magnetometer (VSM) and FTIR spectroscopy.

The detailed characterization information is offered below.

Transmission electron microscopy (TEM) images were collected on a JEM-2100 transmission electron microscopy (JEOL-2100, Japan). The high-resolution TEM, HAADF-STEM images, and the corresponding energy-dispersive X-ray (EDX) mapping were recorded by a JEOL JEM-2100F high resolution transmission electron microscope operating at 200 kV (JEOL JEM-2100F, Japan). AC HAADF-STEM images were collected by using a Titan 80-300 scanning/transmission electron microscope operator at 300 kV, equipped with a probe spherical aberration corrector. The Fe content of the reductants and Fe leaching were determined by a PerkinElmer Optima 5300 DV (PerkinElmer, USA) inductively coupled plasma mass spectrometer system with a radio frequency power of 1300 W. Brunauer-Emmett Teller (BET) surface specific areas were detected at 77 K by N_2 adsorption-desorption isotherms, and the pore diameter was analyzed via Barrett-Joyner-Halenda (BJH) adsorption method (Micromeritics, USA). X-ray diffraction (XRD) patterns were obtained in the range of 20°–75° respectively, using a Cu Kα radiation source (λ = 1.5406 Å) on XRD instrument (Rigaku D/max-RA, Japan). X-ray photoelectron spectroscopy (XPS, ULPAC-PHI, Japan) was conducted on a PHI5000 Versa Probe assembled with a monochromatized Al Kα excitation source ($h\nu$ = 1486.6 eV). The C1s peak (284.6 eV) was used for the calibration of binding energy values. Raman spectroscopy was obtained on a spectrometer (RM-1000, Renishaw, UK) equipped with a He/Ne laser excitation source of 532 nm wavelength. The IR spectra of the samples were recorded at 4 cm^{-1} resolution on a Nicolet 380 FTIR spectrometer using the KBr pellet technique (Nicolet 380 FTIR, USA). Ultroviolet photoelectron spectroscopy (UPS) experiments were conducted at ESCALAB250 (Thermo VG Co., Ltd) using He I (hν = 21.2 eV), where a negative bias voltage of 15 V was applied to the sample to accelerate electrons of low kinetic energy and determine the secondary electron cutoff. The N contents of the reductants were determined on an elemental analyzer (CHN-O-Rapid Heraeus, Germany). The magnetization of the samples was determined by vibrating sample magnetometer (Lake Shore, VSM 7404, USA). Atomic force microscopy (AFM) image was used to characterize the thickness of layer on a Multi

Mode v8 scanning probe microscope (MM-SPM, Bruker, German) with a Scan Asyst Mode. Nyquist plot was recorded by applying a sine wave with amplitude of 5.0 mV over the frequency range from 100 kHz to 0.01 Hz using a CHI-600C electrochemical workstation (CHI-600C, Chenhua, Shanghai).

XAFS spectroscopy

The X-ray absorption fine structure spectra (XAFS) of Fe were performed at the beamline BL1W1B of Beijing Synchrotron Radiation Facility (BSRF), Institute of High Energy Physics (IHEP) of Chinese Academy of Sciences. The storage ring conducted at 2.2 GeV with currents between 100-200 mA. The scanning region of X-ray absorption near edge structure (XANES) and extended X-ray adsorption fine structure (EXAFS) were −50 eV to 50 eV and 50 eV to 1000 eV around the absorption edge, respectively. The XANES data for the proportion of Fe species was conducted by linear combination fitting (LCF) using software Athena. The EXAFS spectra were analyzed using program Artemis to attain the parameters as distance (R), coordination number (CN), and disorder (σ_2). The k^3 weighting, k-range of 2.5-11.2 $Å^{-1}$ and R range of 1-4 Å were applied for EXAFS fitting. The model of Fe foil and $FePO_4$ were used as the fitting path.

Theoretical calculation method. Density functional theory calculation is adopted to further clarify the Cr(VI) adsorption/reduction on Fe-N-C sites, and the electron distribution on the surface of Fe-N-C. The detailed calculation information is provided below.

The model of materials was optimum by Density Functional Theory (DFT), the electron localization function of materials was analyzed by Multiwfn 3.3.9. The model of CN shell was constructed by chemdraw 3D. The model was optimum by Density Functional Theory (DFT) at the B3LYP/6–311 + G* level on the Gaussian 09W software. The calculated results were then analyzed on the Multiwfn 3.3.9 to achieve the information of electron location function values (ELF). After analysis, the exported data of Multiwfn 3.3.9 was visualized by Visual Molecular Dynamics software (VMD, version 1.9.3). The model of $Cr_2O_7^{2-}$ was also constructed on chemdraw3D and the model was optimum by DFT at the B3LYP/6–31G(d, p) level

on the Gaussian 09W software. The obtained results were then analyzed on the Multiwfn 3.3.9 to achieve the frontier electron density value. After analysis, the exported data of Multiwfn 3.3.9 was visualized by VMD.

Reduction Performance Evaluation. Typically, 10.4 mg/L of Cr(VI) solution (200 mL) was added into 250 ml conical flasks and pH was preset to be 2.0 with diluted HCl solution. Then, the flasks were transferred into a shaker with a rate of 200 rpm. Finally, the reductant was added to evoke the reaction. The sample was collected with syringe at certain intervals and filtered with a 0.45 μm filter to remove reductant particles for detection. The reaction temperature was kept at 25^{o}C in whole reaction processes.

Reusability test experiment. To test reductant reusability, reductant reuse was conducted in six parallel experimental groups. In each group, 8 mg of reductant was added to the reactor containing 200 mL of Cr(VI) solution (10.4 mg/L) with pH of 2.0. The reaction was conducted and samples were taken at different time intervals for further determined. In parallel, the used catalyst was prepared under same reaction conditions but without sampling. After reaction for 120 min, the used reductant was recovered by magnetic separation followed by washing with deionized water and dried at 60 ^{o}C for 12 h. The recovered reductant was regenerated by carbothermic reaction at 900 ^{o}C for 2h. The regenerated reductant was subjected to next reaction cycle. As for the carbon replenishment, the nonrenewable Fe reductant and aniline were placed in quartz crucibles for PANI encapsulation using CVD process, and following pyrolysis (with reference to mentioned CVD and pyrolysis processes).

Hydroponic mungbean experiment. Initially, full and even seeds are selected for germinated by incubation at 28±1 ^{o}C for 24 h in petri dishes. When all the seeds of blank group have sprouted, the germinant rates of tested groups are calculated. Following, the rooted seeds are transferred to the engraftment basket for further cultivation in insect-free and visible-light glass house. It should be noted that the seed coat is removed gently prior to cultivation. The used nutrient solution is preset to neutral.

Analytical methods

The concentration of Cr(VI) was detected spectrophotometrically using 1,5-diphenylcarbazide as the color agent. The concentration of total Cr was determined with atomic absorption spectroscopy (AAS) on Perkin-Elmer 5100. The initial activity was used to evaluate reductant activity, which is defined as reductant-mass normalized removal rate of Cr(VI) within 6 min. Removal capacity was used to evaluate Cr(VI) removal amount on the whole reaction process (120 min).

$$Initial\ activity = \frac{C_0 - C_t}{m_{reductant} \times t} \qquad \text{Equation 1}$$

$$Removal\ capacity = \frac{(C_0 - C_{120})V}{m_{reductant}} \qquad \text{Equation 2}$$

where $C_0\ (mg/L)$is initial Cr(VI) concentration and $C_t(mg/L)$ is Cr(VI) concentration after reaction for t min, V is the volume of reaction solution.

The average particle size of reductant was calculated on the basis of surface area weighted diameter:

$$\bar{d}_s = \frac{\sum n_i d_i^3}{\sum n_i d_i^2} \qquad \text{Equation 3}$$

where n_i is the counting number of Fe particles with diameter of d_i.

Supplementary Figures

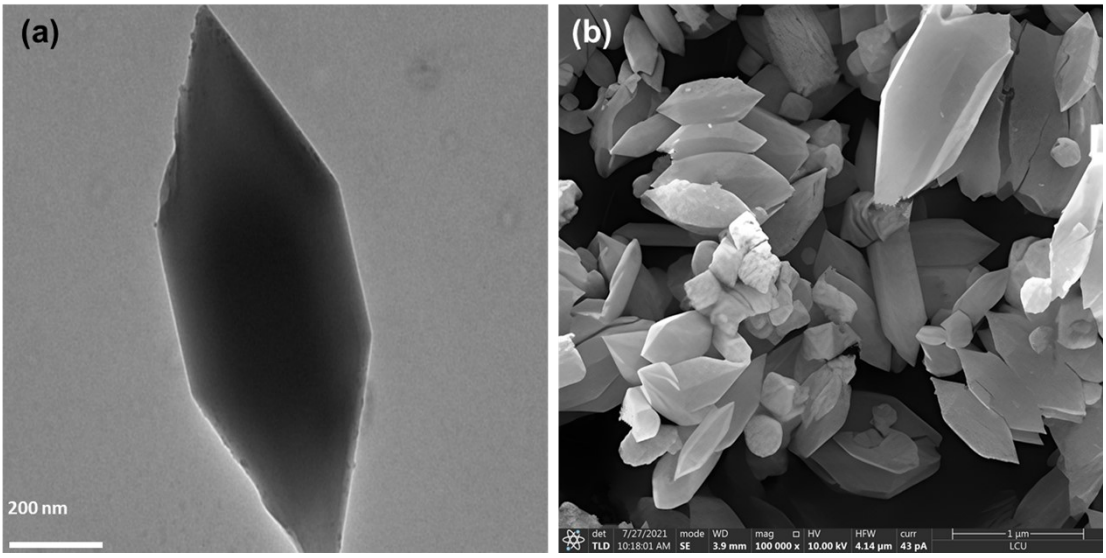

Figure S1 TEM (a) and SEM image of NH_2-MIL-101(Fe).

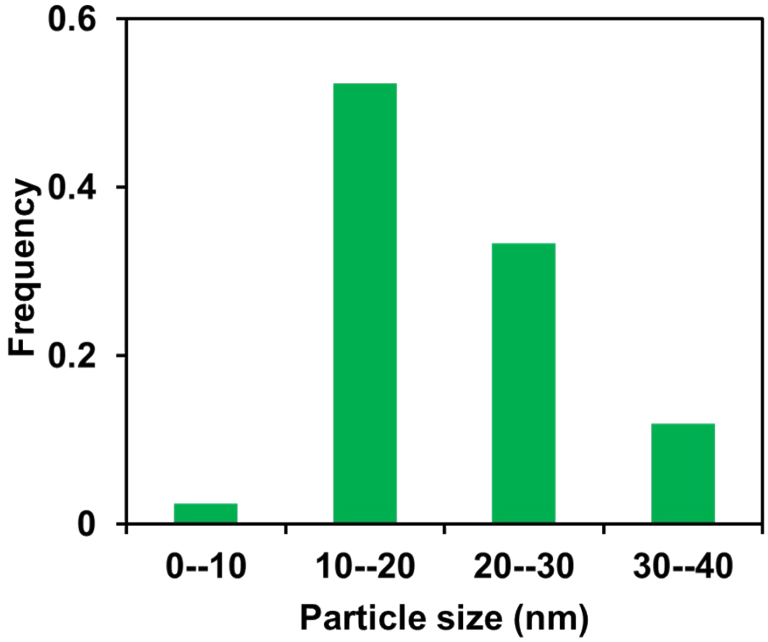

Figure S2 Particle distribution of Fe particles on Fe_{NPs}/CN.

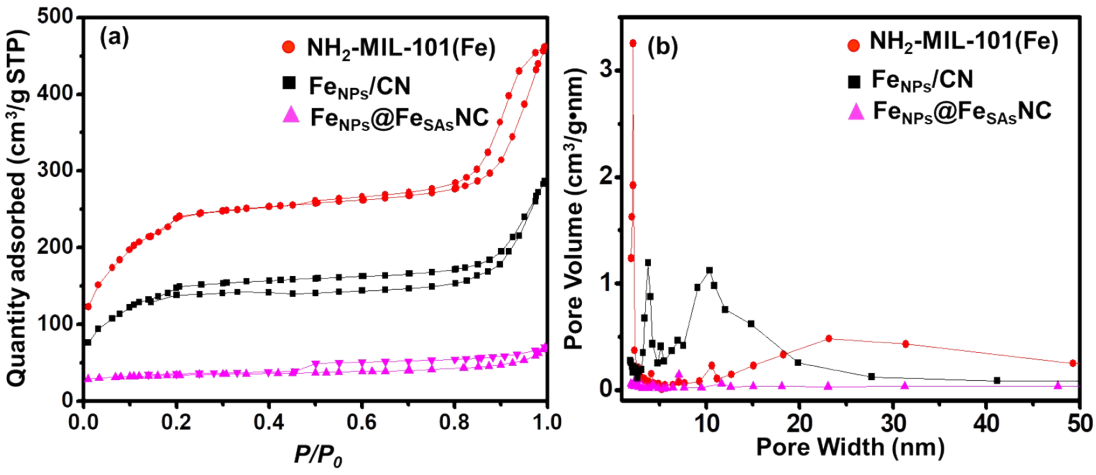

Figure S3. The N_2 desorption-adsorption isotherm curves (a) and pore size distribution (b).

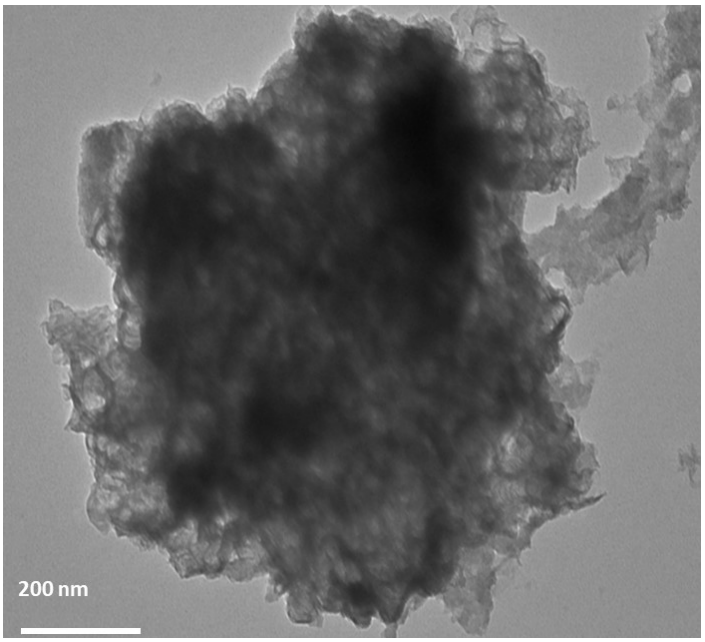

Figure S4 TEM image of Fe_{NPs}/CN@PANI.

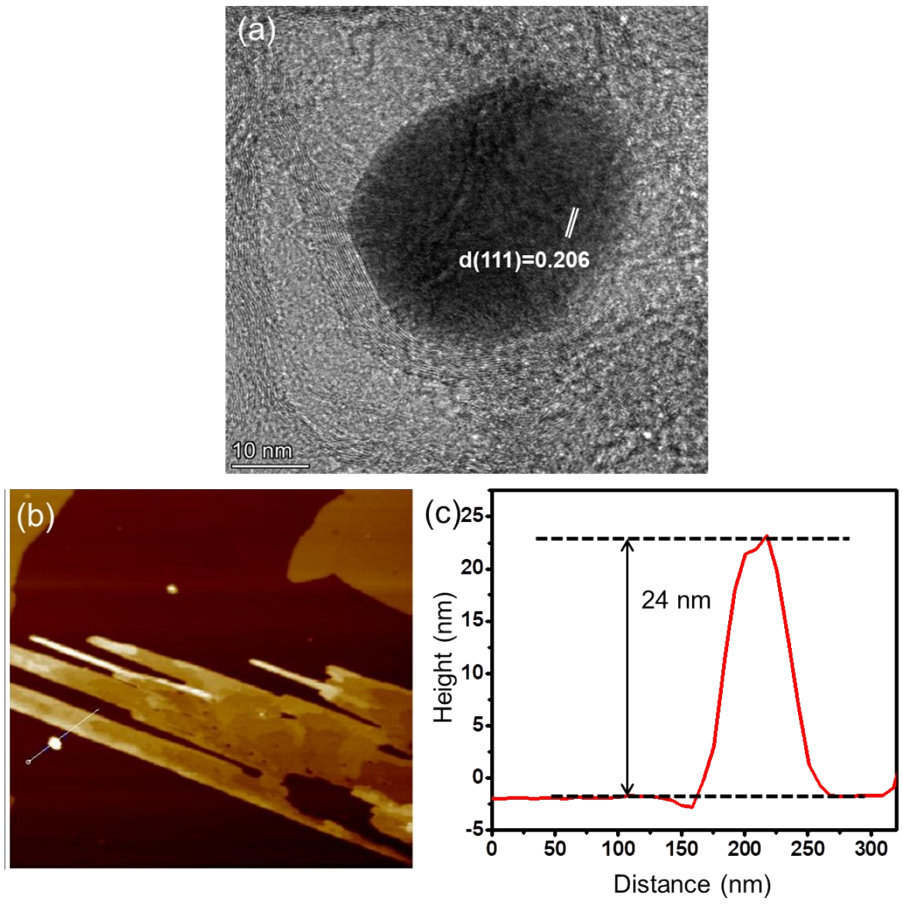

Figure S5 (a) HR-TEM image of Fe particle over Fe_{NPs}/CN, (b) AFM image of Fe_{NPs}/CN and corresponding height profile.

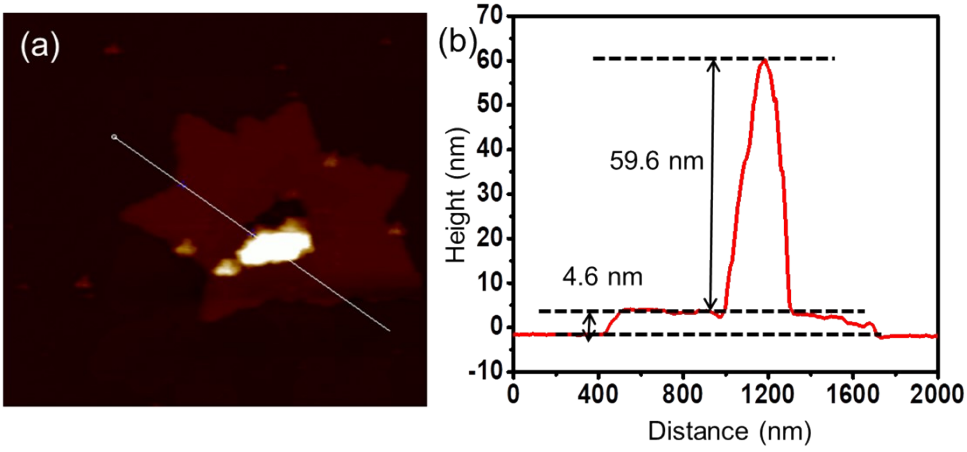

Figure S6 (a) AFM image of Fe_{NPs}@Fe_{SAs}NC and (b) corresponding height profile.

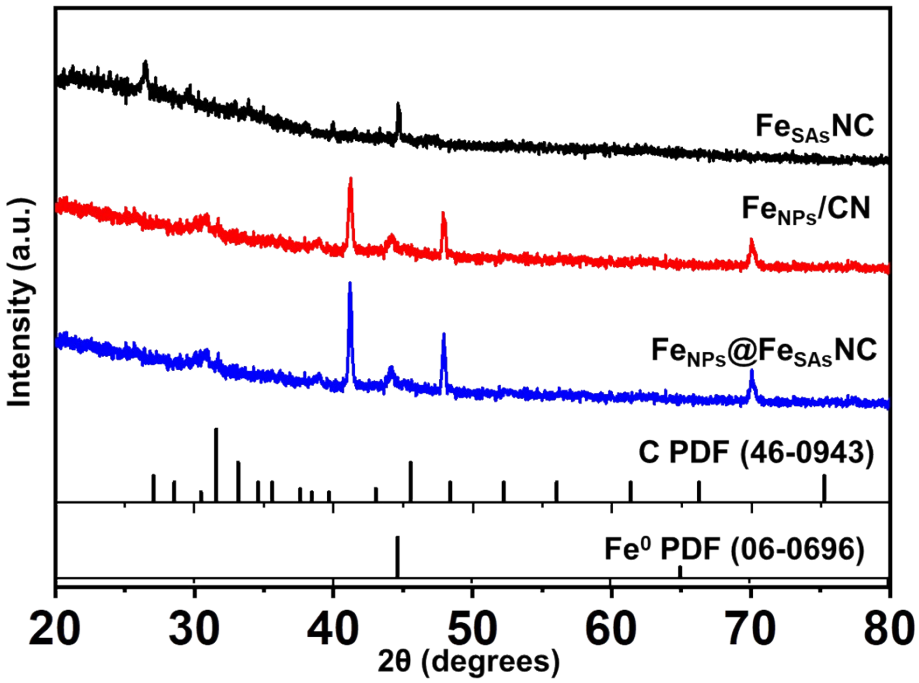

Figure S7 XRD pattern of Fe_{NPs}@Fe_{SAs}NC, Fe_{NPs}/CN and Fe_{SAs}NC.

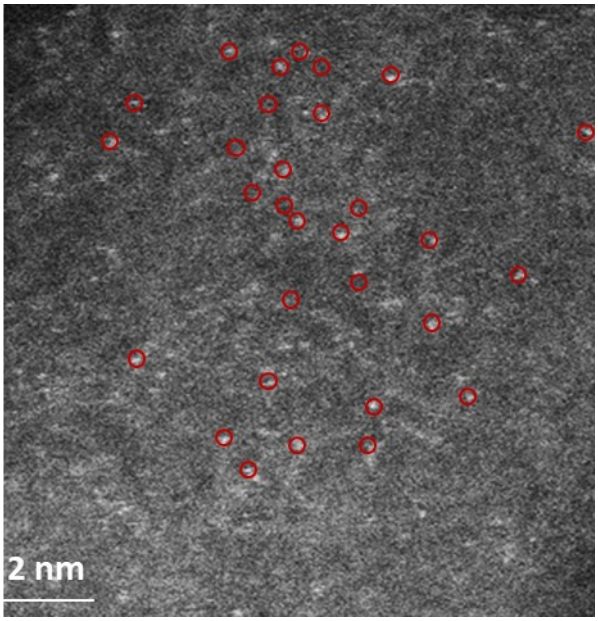

Figure S8 AC HAADF-STEM images of Fe_{SAs}NC.

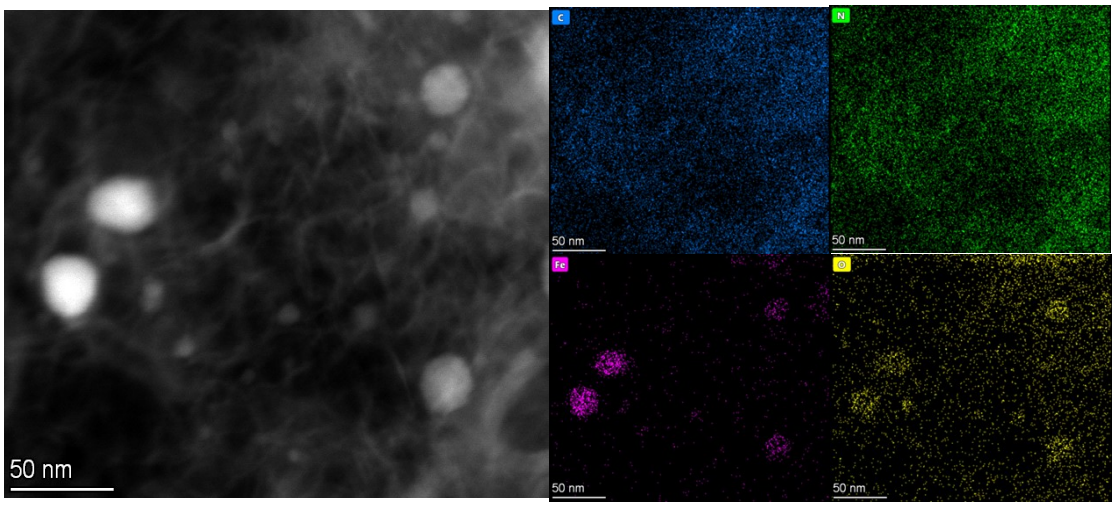

Figure S9 HAADF-STEM and C, N, Fe, O EDS mapping images of Fe_{NPs}/CN.

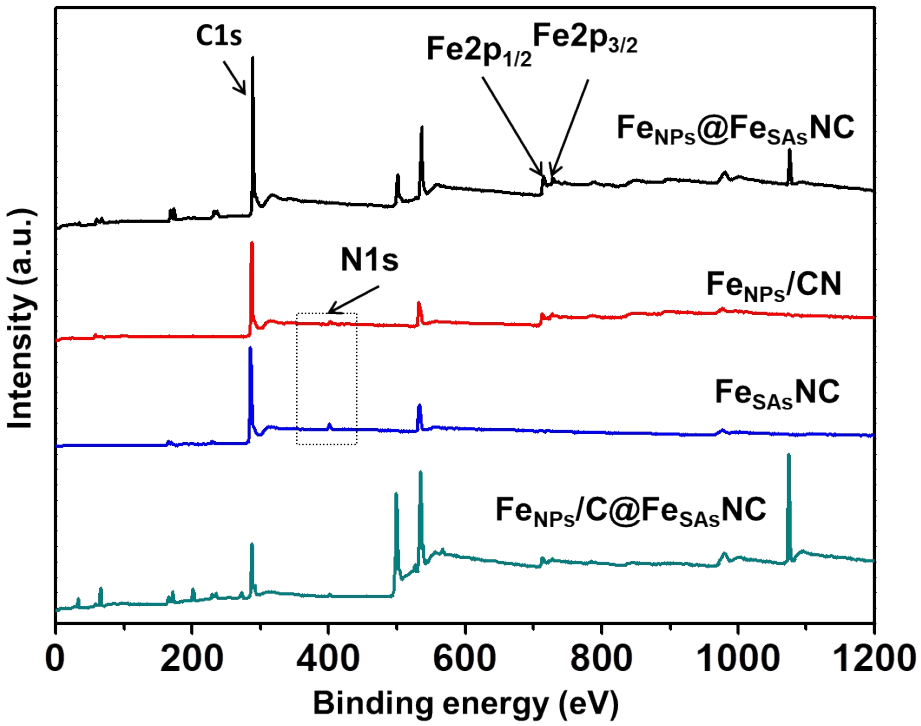

Figure S10 Full scanning XPS spectra of materials.

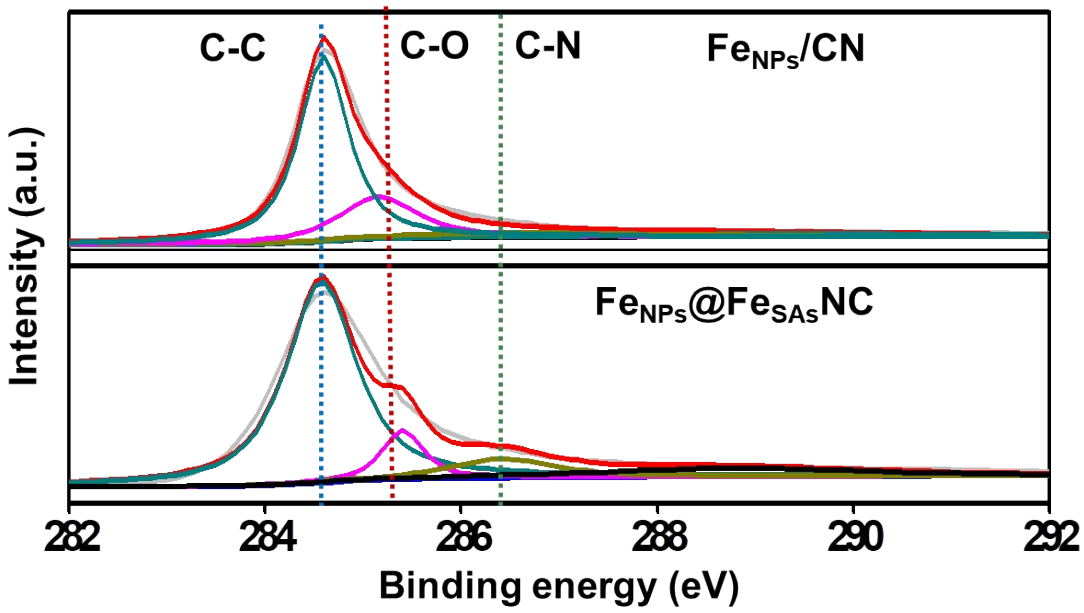

Figure S11 The survey XPS spectra of C1s element for Fe_{NPs}/CN and Fe_{NPs} @Fe_{SAs}NC.

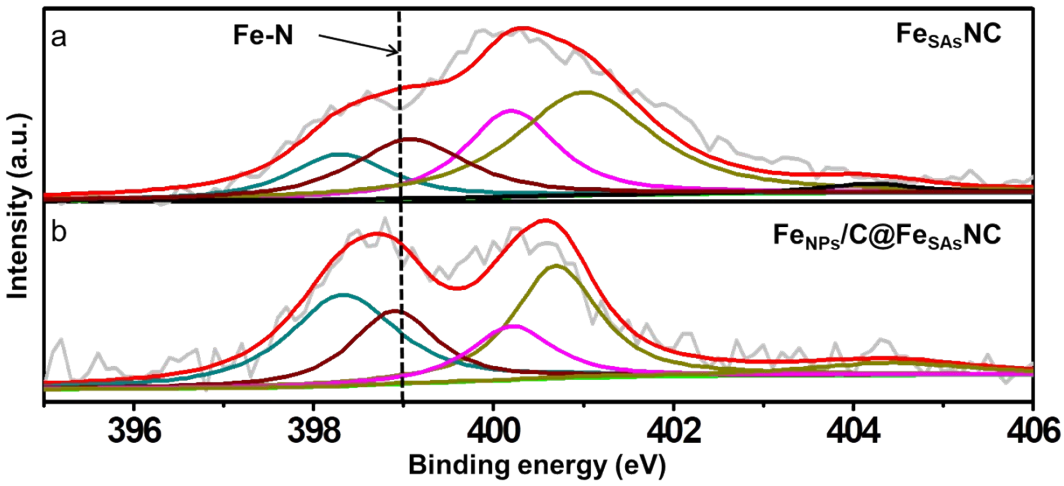

Figure S12 The survey XPS spectra of N1s element for Fe_{SAs}CN and Fe_{NPs}/C@Fe_{SAs}NC.

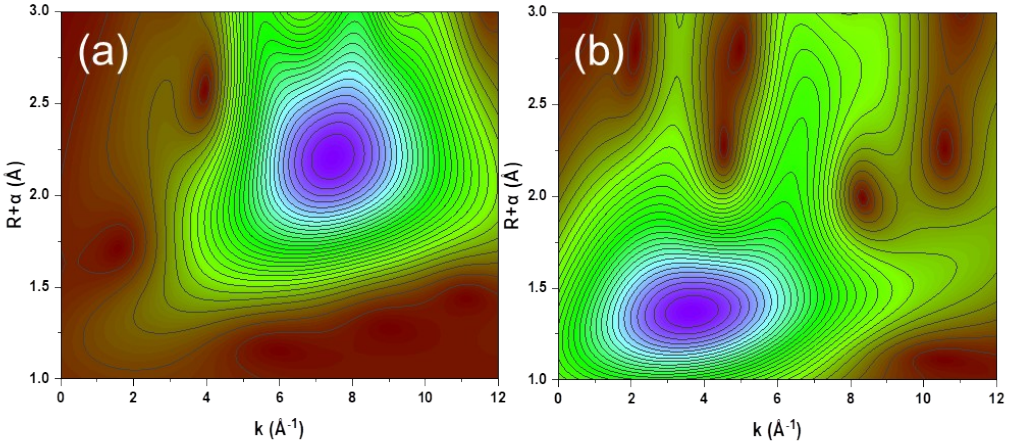

Figure S13 The wavelet transforms (WT)-EXAFS of the scattering Fe atoms in k space referring in Fe foil (a), FePc (b).

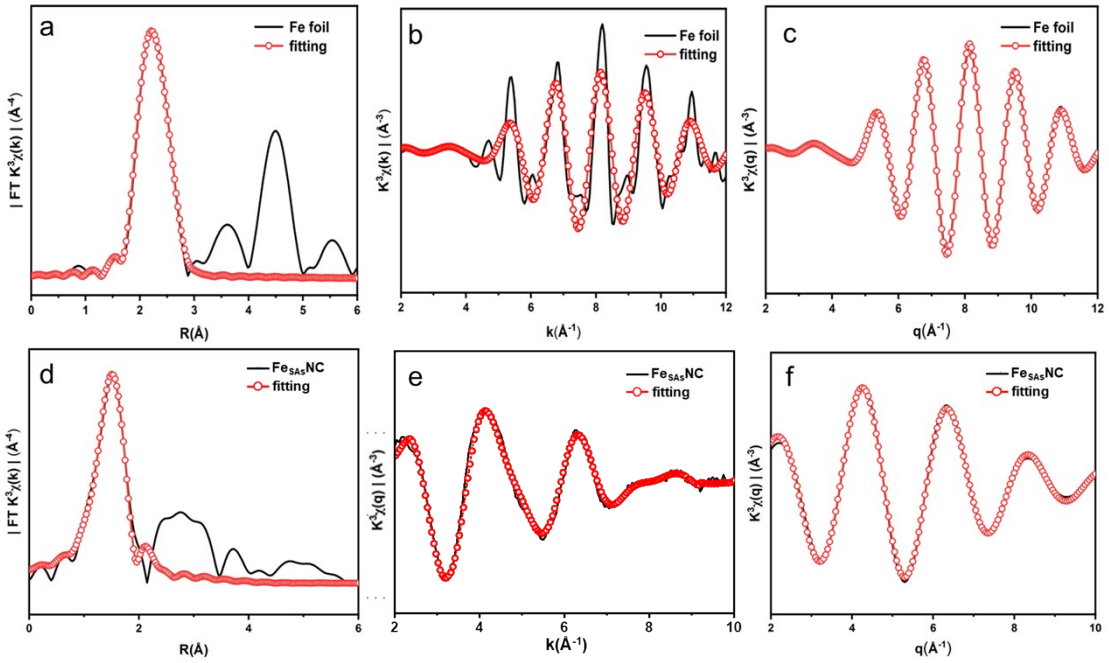

Figure S14 FT-EXAFS fitting curves of Fe foil at R (a), k (b) and (c) q space and $Fe_{SAs}NC$ at R (d), k (e) and (f) q space.

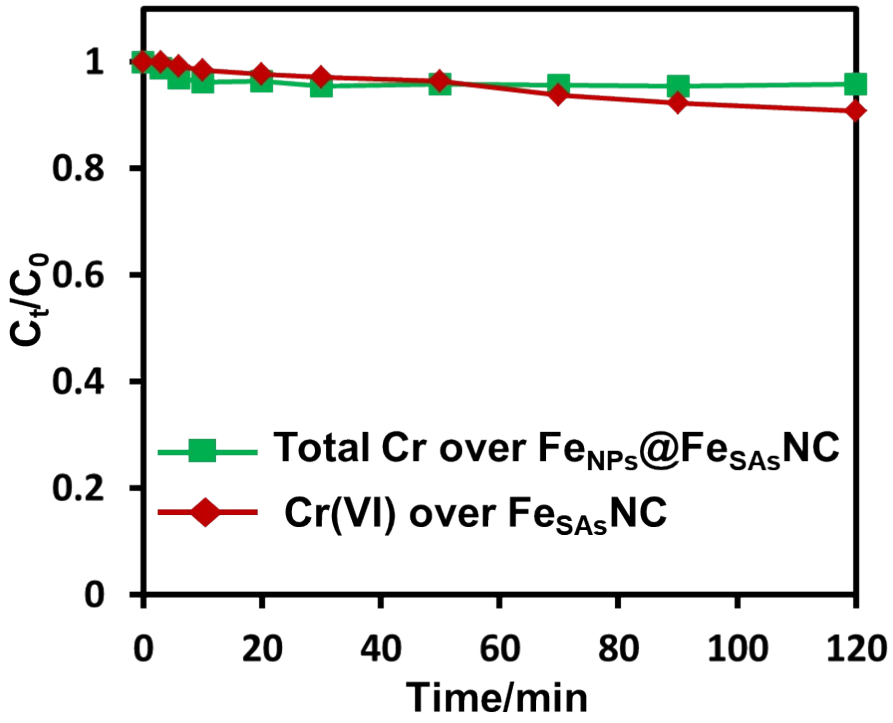

Figure S15 The total Cr concentration over Fe_{NPs}@Fe_{SAs}NC. Reaction condition: reductant dosage=40 mg/L, initial Cr(VI) concentration=10.4 mg/L, pH=2.0.

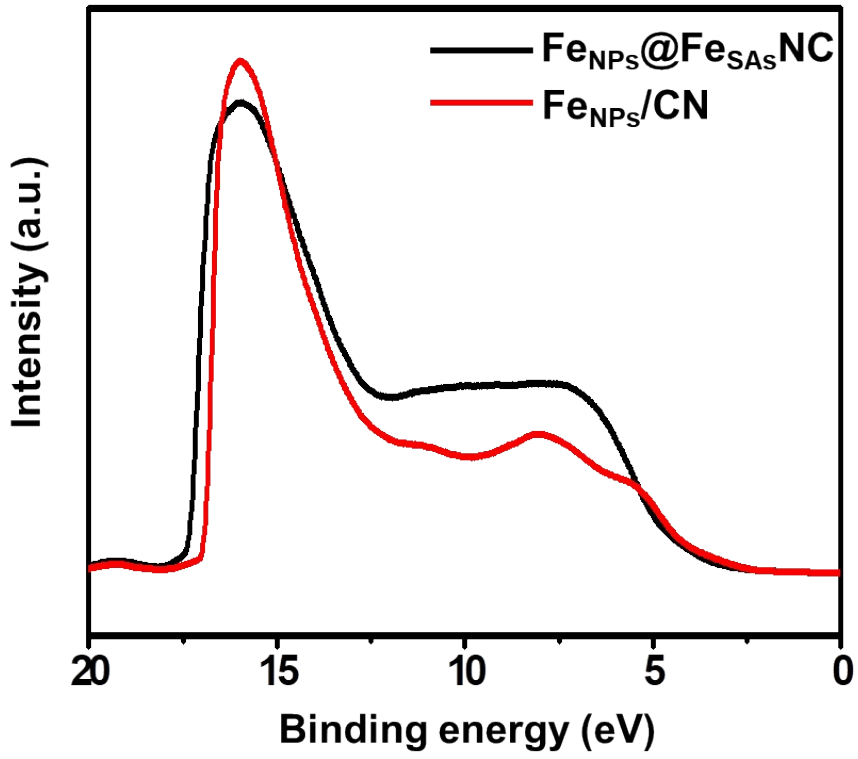

Figure S16 UPS spectra of Fe_{NPs}@Fe_{SAs}NC and Fe_{NPs}/CN.

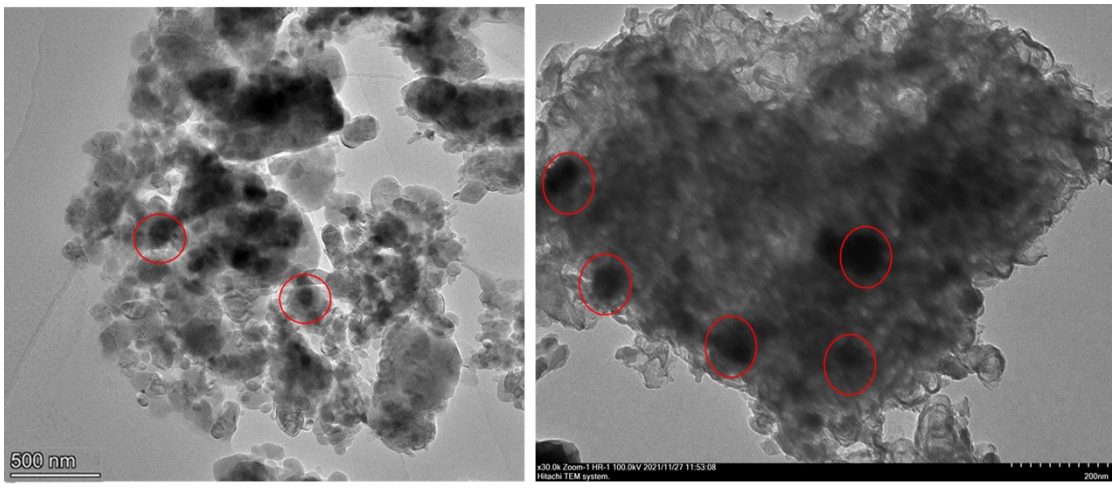

Figure S17 TEM images of Fe_{NPs}@Fe_{SAs}NC in a broad dimension.

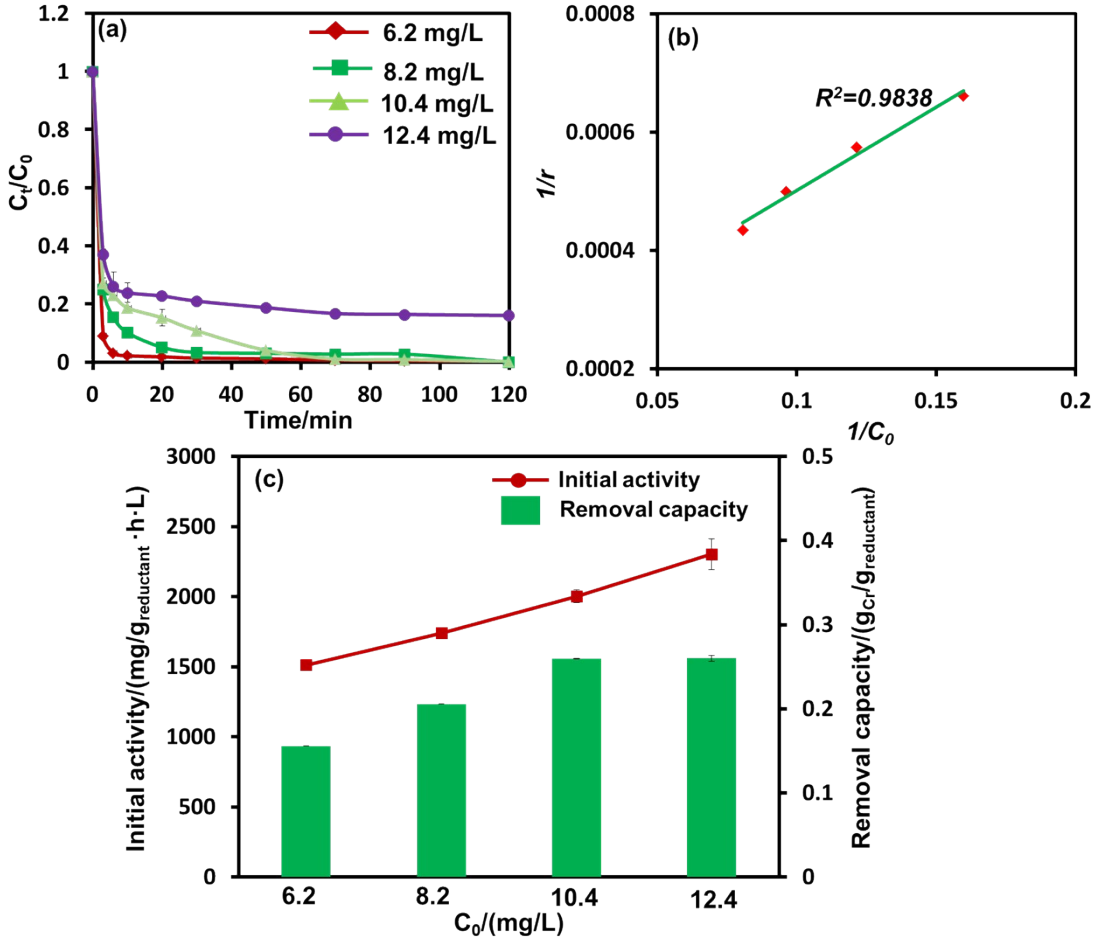

Figure S18 (a) Influence of initial Cr(VI) concentration of Cr(VI) reduction over Fe_{NPs}@Fe_{SAs}NC, (b) linear plot of $1/r$ versus $1/C_0$ and (c) corresponding initial activity, removal capacity. Reaction condition: reductant dosage=40 mg/L, pH=2.0.

The effect of initial Cr(VI) concentration on activity are presented in Figure S24(a). The initial activity of Fe_{NPs}@Fe_{SAs}NC increased from 1511 mg/g reductant·h·L to 2303 mg/g reductant·h·L with increase of initial Cr(VI) from 6.2 mg/L to 12.4 mg/L (Figure S24(c)). The reaction data were fitted to Langmuir-Hinshelwood model, which was described as follows,

$$r_0 = k\theta_s = k\frac{bC_0}{1+bC_0}$$

$$\frac{1}{r_0} = \frac{1}{kbC_0} + \frac{1}{k}$$

where r_0 is the initial reduction rate at Cr(VI) concentration of C_0, θ_s is the coverage of Cr(VI) adsorption on the $Fe_{NPs}@Fe_{SAs}NC$ surface, k is the reaction rate constant and b is the equilibrium constant for bromate adsorption.

The plot of $1/r_0$ versus $1/C_0$ is presented in Figure 24(b) and a good linear relationship between $1/r_0$ and $1/C_0$ was obtained with $R^2>0.95$. The fitting results indicated that Cr(VI) reduction could be well described by the Langmuir-Hinshelwood model and the conversion of adsorbed Cr(VI) on $Fe_{NPs}@Fe_{SAs}NC$ surface was the rate controlling step, confirming the crucial role of Cr(VI) adsorption on reduction.

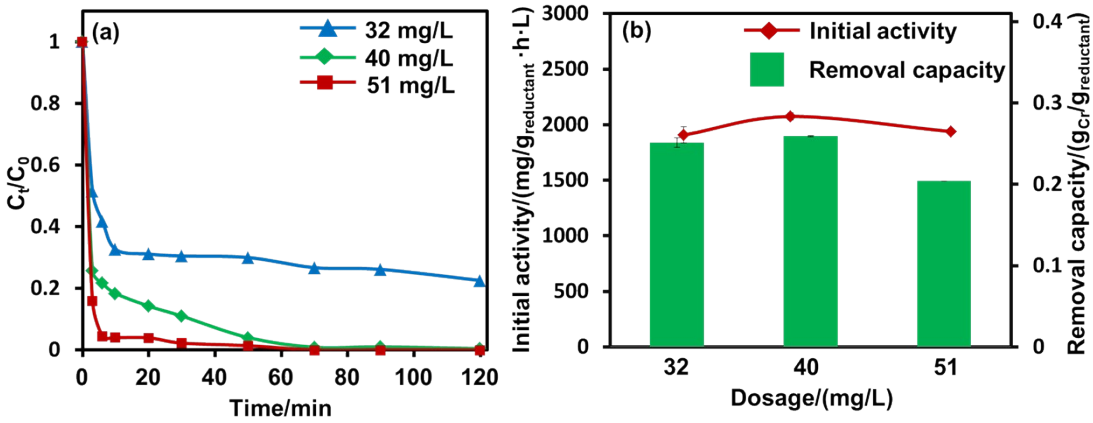

Figure S19 (a) Cr(VI) reduction over varied Fe_{NPs}@Fe_{SAs}NC dosage, (b) corresponding initial activity and removal capacity. Reaction condition: initial Cr(VI) concentration=10.4 mg/L, pH=2.0.

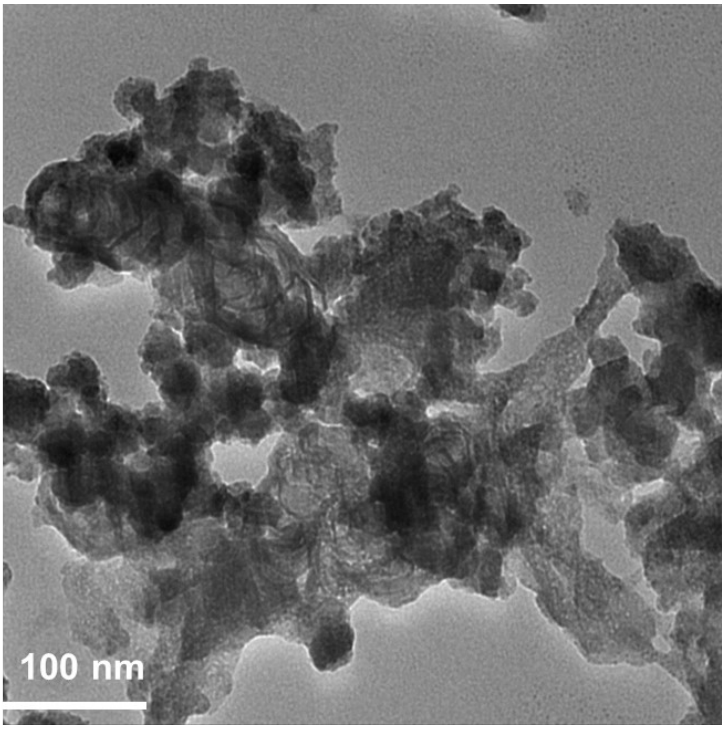

Figure S20 TEM images of regenerated $Fe_{NPs}@Fe_{SAs}NC$.

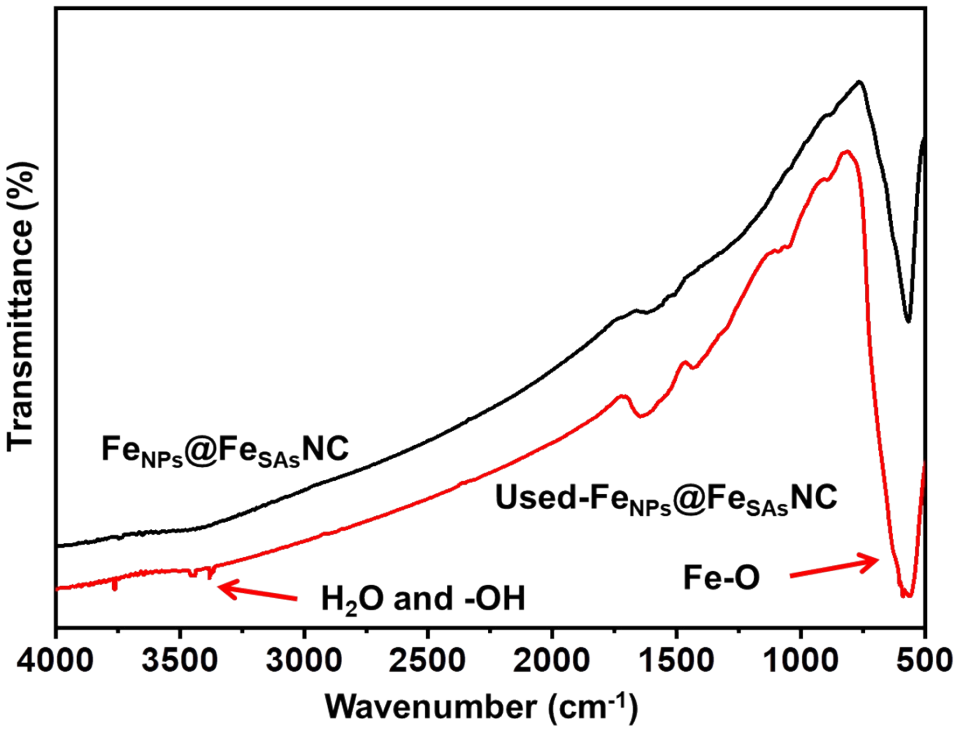

Figure S21 FT-IR spectrum of $Fe_{NPs}@Fe_{SAs}NC$ and used- $Fe_{NPs}@Fe_{SAs}NC$.

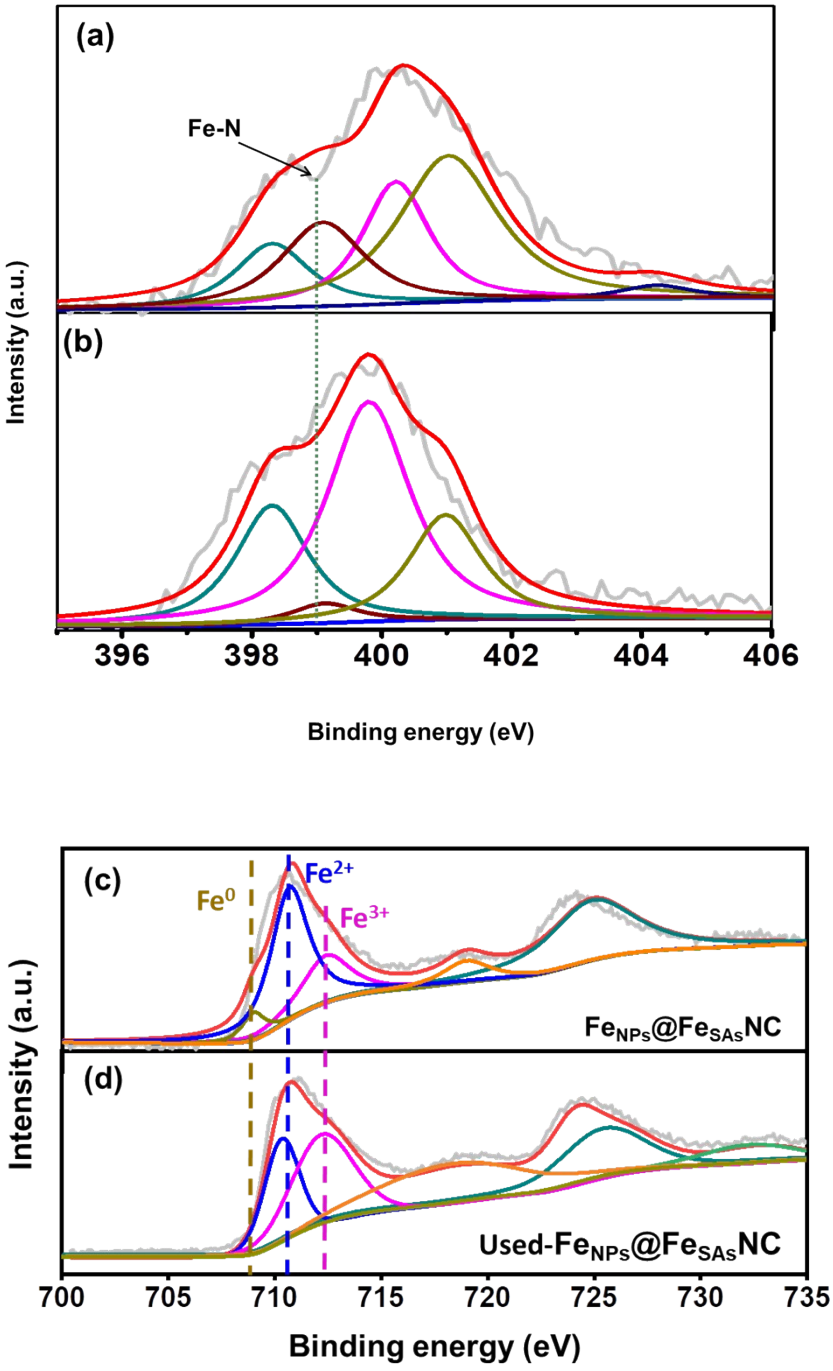

Figure S22 The XPS spectra of N1s (a) and Fe2p (c) of original $Fe_{NPs}@Fe_{SAs}NC$ and N1s (b) and Fe2p (d) of used and regenerated $Fe_{NPs}@Fe_{SAs}NC$ for three times.

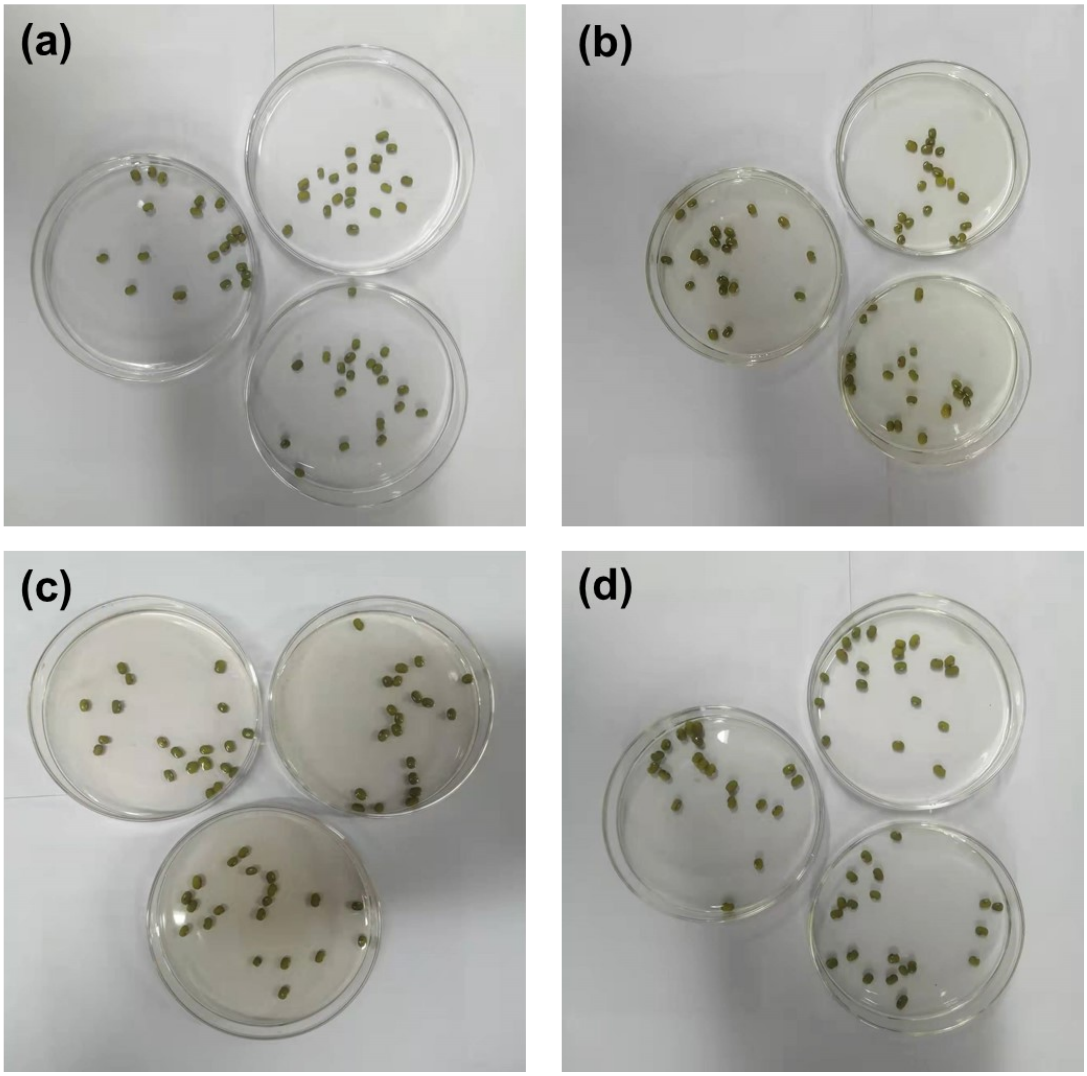

Figure S23 The initial stage of hydroponic mungbean for sprout in DI (a), Cr(VI) solution (b), Cr+ Fe_{NPs} /CN (c), Cr+ Fe_{NPs}@Fe_{SAs}NC (d).

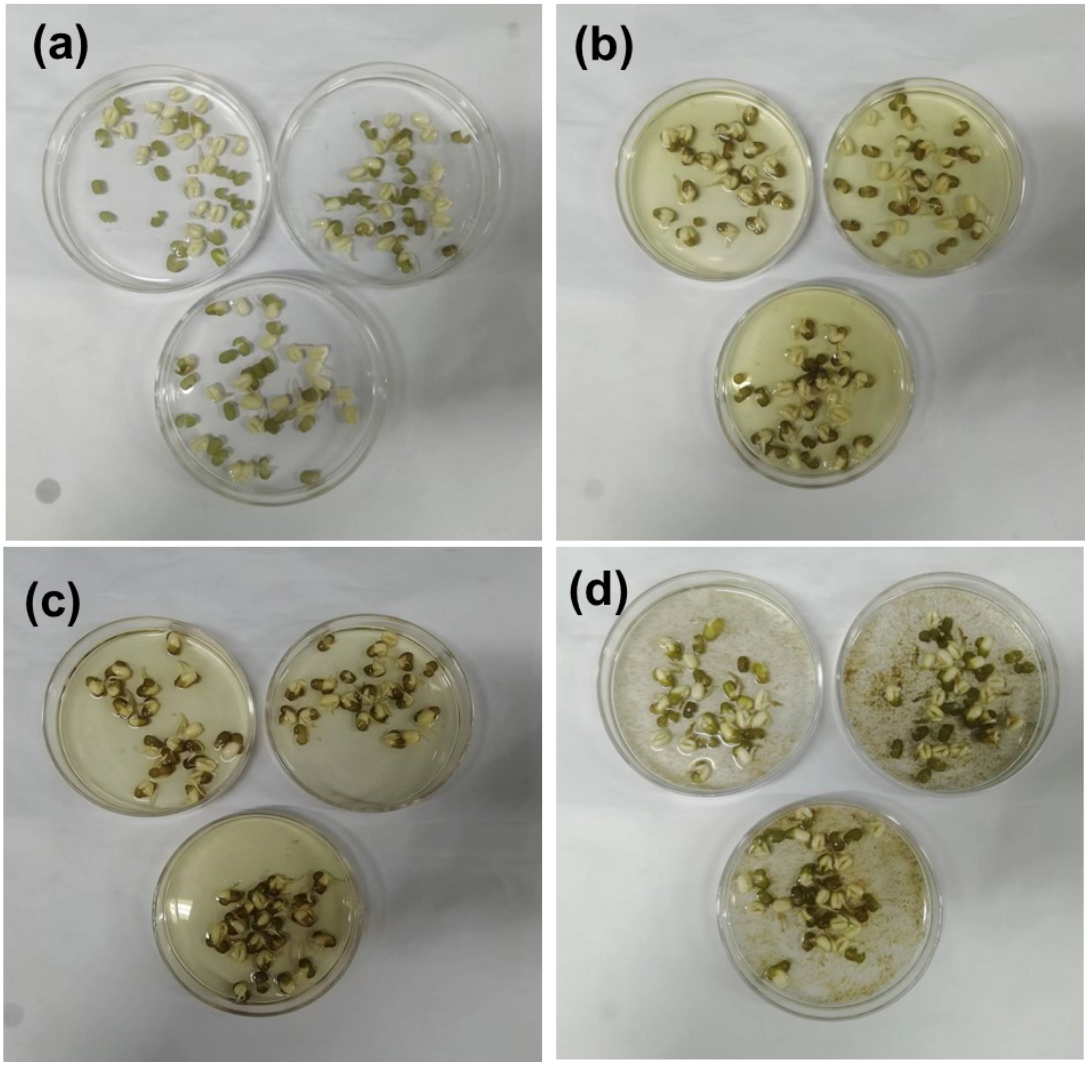

Figure S24 Germinant rates of mungbean experiment in DI (a), Cr(VI) solution (b), Cr+ Fe_{NPs} /CN (c), Cr+ Fe_{NPs}@Fe_{SAs}NC (d).

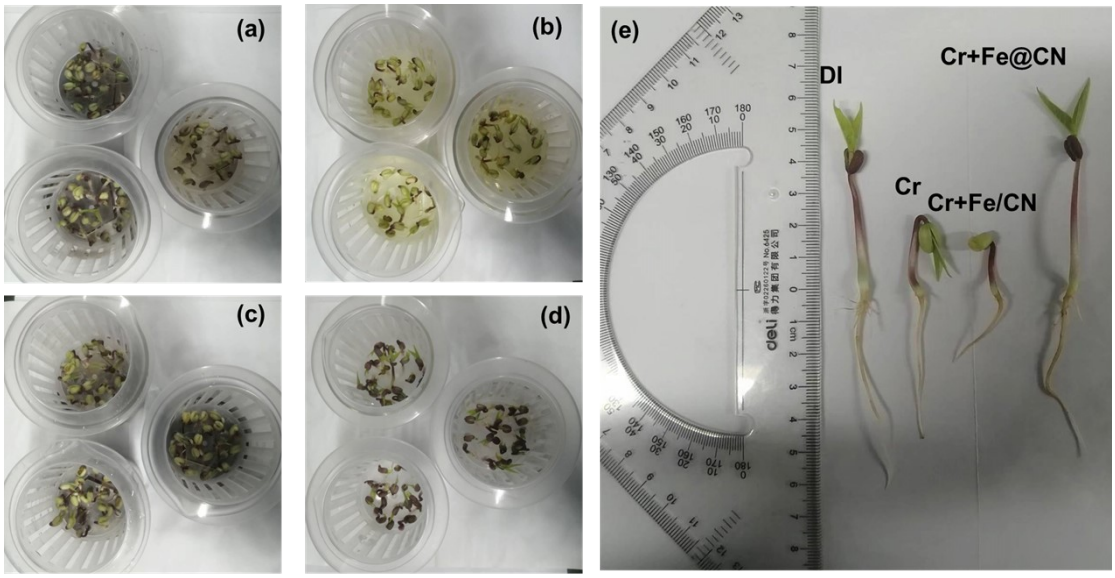

Figure S25 Growing statuses of mungbean seedling in DI (a), Cr(VI) solution (b), Cr+ Fe_{NPs} /CN (c), Cr+ Fe_{NPs}@Fe_{SAs}NC (d). at 4th day.

The 5th day:

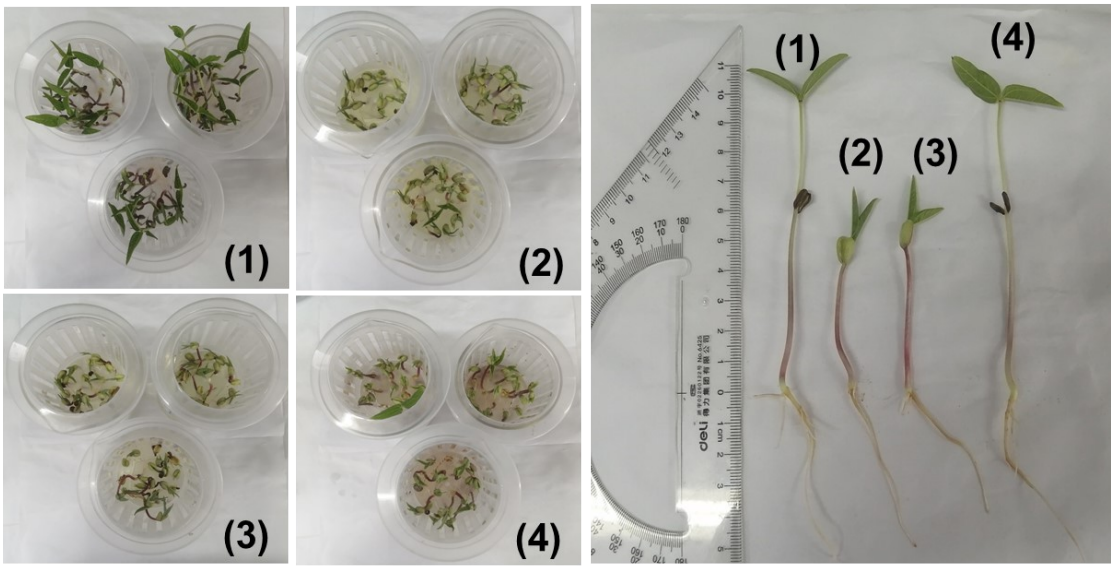

The 6th day:

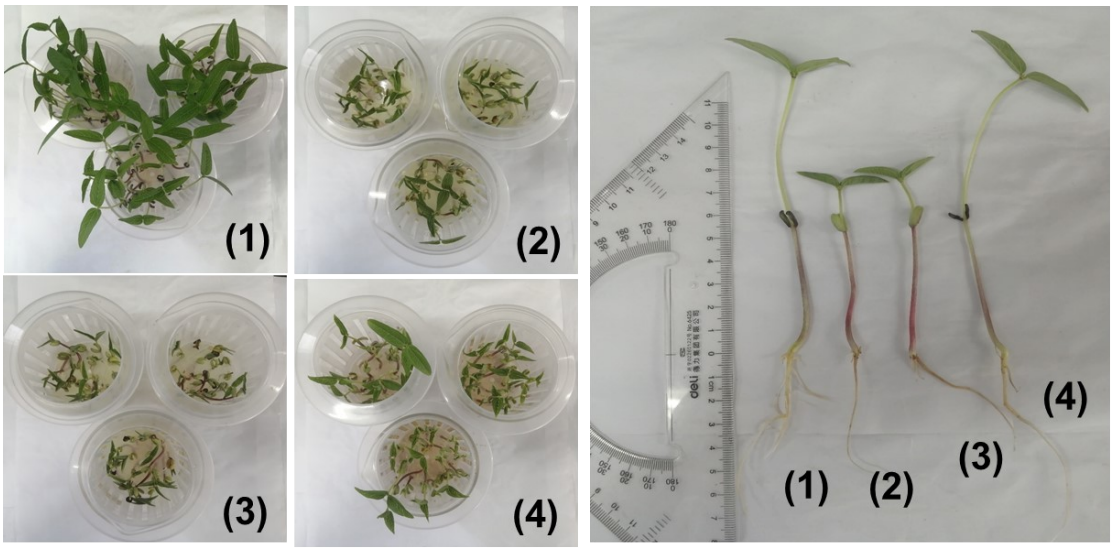

The 7th day

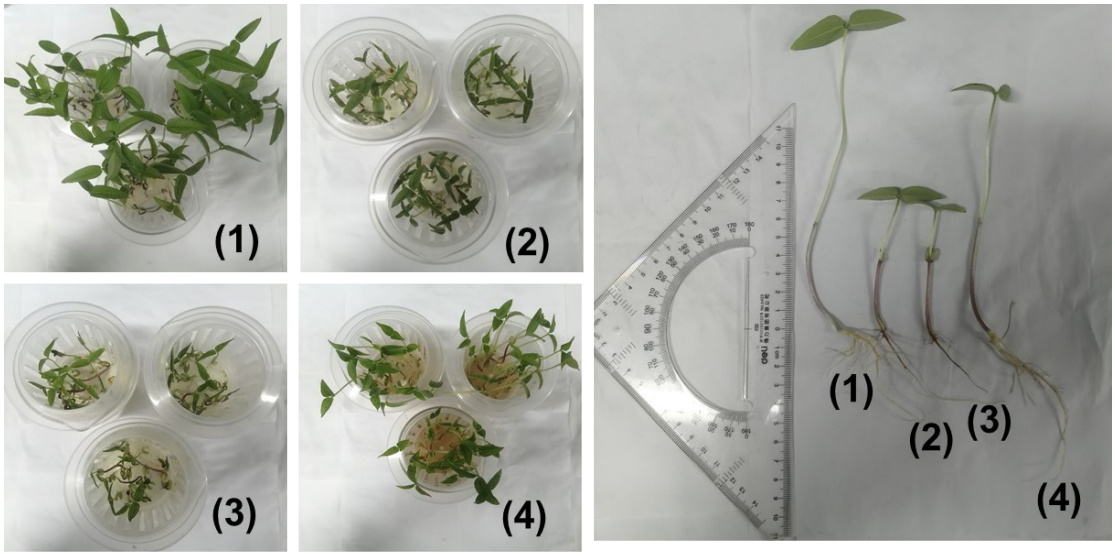

The 8th day

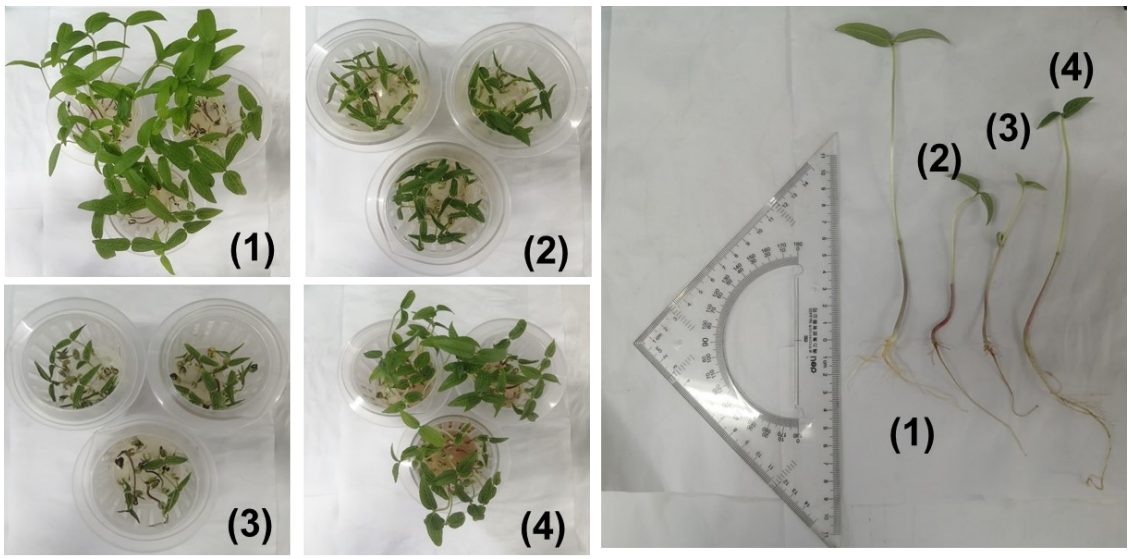

Figure S26 Detailed growing statuses of mungbean in (1) DI, (2) Cr(VI), (3) Cr+ Fe_{NPs} /CN, (4) Cr+ Fe_{NPs}@Fe_{SAs}NC.

Table S1 Structure parameters of NH_2-MIL-101(Fe), Fe_{NPs}/CN and Fe_{NPs}@Fe_{SAs}NC.

Sample	S_{BET}[a] (m^2/g)	V_t[b] (m^3/g)	V_{micro}[c] (m^3/g)	D_{BJH}[d]
NH_2-MIL-101(Fe)	740.0	0.67	0.66	3.60
Fe_{NPs}/CN	342.6	0.23	0.17	9.42
Fe_{NPs}@Fe_{SAs}NC	100.9	0.09	0.04	3.64

[a] calculated by Brunauer-Emmett-Teller (BET) method

[b] obtained at P/P_0=0.995

[c] calculated by *t*-plot method

[d] from BJH method

Table S2 The atomic and mass fraction of Fe materials from EDS-Mapping.

Sample	Atomic fraction (%)				Mass fraction (%)			
	C	N	O	Fe	C	N	O	Fe
Fe_{NPs}/CN	90.92	1.03	2.29	5.76	75.48	0.03	2.51	21.99
Fe_{NPs}@Fe_{SAs}NC	6.39	1.83	57.56	34.22	2.62	0.87	31.39	65.12

Table S3 Element content analysis.

Sample	Surface atom ratio (%)[a]			Fe content (wt%)[b]	N content (wt%)[c]
	Fe	N	C		
Fe_{NPs}@Fe_{SAs}NC	3.49	3.25	93.27	28.9	3.12
Fe_{NPs}/CN	5.32	2.57	92.12	31.5	2.57
Fe_{NPs}/C@Fe_{SAs}NC	3.47	0.82	95.71	43.8	1.21

[a] measured by XPS

[b] measured by ICP-MS

[c] measured by Element analyzer

Table S4 Binding energies and atomic percentages of different Fe species in Fe_{NPs}/CN and Fe_{NPs}@Fe_{SAs}NC from Fe 2p XPS spectra.

Classification	Fe_{NPs}/CN			Fe_{NPs}@Fe_{SAs}NC		
	Fe^0	Fe^{2+}	Fe^{3+}	Fe^0	Fe^{2+}	Fe^{3+}
Binding Energy (eV)	708.5	710.8	726.3	708.5	713.0	730.3
Proportion (%)	4.7	59.0	36.3	8.1	63.6	28.6

Table S5. Structural parameters extracted from the Fe K-edge EXAFS fitting. (S_0^2=0.739)

sample	**Scattering pair**	**CN**	**R(Å)**	**σ^2(10^{-3}Å^2)**	**ΔE_0(eV)**	**R factor**
Fe_{NPs}@Fe_{SAs}NC	Fe-N	5.16	1.99	10.0	1.04	0.008
Fe_{SAs}NC	Fe-N	4.04	2.01	12.8	2.99	0.008
Fe foil	Fe-Fe	8*	2.46	5.4	4.19	0.006

S_0^2 is the amplitude reduction factor; CN is the coordination number; R is interatomic distance (the bond length between central atoms and surrounding coordination atoms); σ^2 is Debye-Waller factor (a measure of thermal and static disorder in absorber-scatterer distances); ΔE_0 is edge-energy shift (the difference between the zero kinetic energy value of the sample and that of the theoretical model). R factor is used to value the goodness of the fitting.

* This value was fixed during EXAFS fitting, based on the known structure.

Error bounds that characterize the structural parameters obtained by EXAFS spectroscopy were estimated as N ± 20%; R ± 1%; σ^2 ± 25%; ΔE_0 ± 10%.

Fe_1NC (FT range: 2.0-10.8 Å^{-1}; fitting range: 1-2 Å)
Fe foil (FT range: 2.0-12.0 Å^{-1}; fitting range: 1-3 Å)

Table S6. Comparison of Cr(VI) removal capacity over Fe-based materials.

Fe-based material	**pH**	**Fe content (wt.%)**	**$g_{Cr}/g_{Reductant}$**	**Reference**
$Fe_{NPs}@Fe_{SAs}NC$	2.0	28.9	0.259	This work
LZVI	6.28	>99	4×10^{-4}	[1]
OX-ZVI	5.2	98.5	6×10^{-3}	[2]
AMBBC-nZVI	5	50	0.057	[3]
Hollow ZVI	3	Not provided	0.02	[4]
ZVI/HAP	5.25	50.2	0.048	[5]
nZVI/graphene	2.0	Not provided	0.046	[6]

Reference:

(1) Y. Hu, X. Peng, Z. Ai, F. Jia, L. Zhang, Liquid nitrogen activation of zero-valent iron and its enhanced Cr(VI) removal performance. Environ. Sci. Technol. 2019, 53: 8333−8341.

(2) Y. Hu, G. Zhan, X. Peng, X. Liu, Z., F. Jia, S. Cao, F. Quan, W. Shen, L. Zhang. Enhanced Cr(VI) removal of zero-valent iron with high proton conductive $FeC_2O_4\cdot2H_2O$ shell. Chem. Eng. J., 2020, 389: 124414.

(3) X. Zhou, Y. Wang, H. Liu, Y. Zhang, Y. Fan, S. Mo, H. Li, J. Wang, H. Lin, Novel amino-modified bamboo-derived biochar-supported nano-zero-valent iron (AMBBC-nZVI) composite for efficient Cr(VI) removal from aqueous solution. Environ. Sci. Pollut. Res., 2023, 30: 119935–119946.

(4) C. Gao, B.Wang, X. Li, Y. Zhang, T. Qu, X. Du, J. Zheng, J. Feng, Removal of Cr(VI) by hollow micron zero-valent iron in groundwater containing different ions: Mechanisms and mineralized products. Process Saf. Environ., 2023, 173: 614-626.

(5) W. Yang, D. Xi, C. Li, Z. Yang, Z. Lin, M. Si, “In-situ synthesized” iron-based bimetal promotes efficient removal of Cr(VI) in by zero-valent iron-loaded hydroxyapatite. J. Hazard. Mater., 2021, 420: 126540.

(6) P. P. Mon, P. P. Cho, L. Chanadana, K.V. Ashok Kumar, S. Dobhal, T. Shashidhar, G. Madras, C. Subrahmanyam, Bio-waste assisted phase transformation of

Fe_3O_4/carbon to nZVI/graphene composites and its application in reductive elimination of Cr(VI) removal from aquifer. Sep. Purif. Technol., 2023, 306: 122632.

Table S7 The growing parameters of mung bean at 9th.

Culture solution	**Seed number**	**Germinantion rates (%) (10 h)**	**Survival rate (%) (9th day)**	**Plant length (cm) (9th day)**
DI	20	100	100	27.05
Cr(VI)	20	81.7	100	13.24
Cr + Fe_{NPs}/CN	20	86.7	100	11.16
Cr + Fe_{NPs}@Fe_{SAs}NC	20	93.3	100	25.95